The structure, phase transition and molecular dynamics of $[C(NH_2)_3]_3[Sb_2Br_9]$

2005 J. Phys.: Condens. Matter 17 2509

(http://iopscience.iop.org/0953-8984/17/15/021)

INSTITUTE OF PHYSICS PUBLISHING JOURNAL OF PHYSICS: CONDENSED MATTER

J. Phys.: Condens. Matter **17** (2005) 2509–2528 doi:10.1088/0953-8984/17/15/021

The structure, phase transition and molecular dynamics of $[C(NH_2)_3]_3[Sb_2Br_9]$

P Szklarz[1], J Zaleski[2], R Jakubas[1,4], G Bator[1], W Medycki[3] and K Falińska[3]

[1] Faculty of Chemistry, University of Wrocław, Joliot-Curie 14, 50–383 Wrocław, Poland
[2] Institute of Chemistry, University of Opole, Oleska 48, 45-951 Opole, Poland
[3] Institute of Molecular Physics, PAS, M Smoluchowskiego 17, 60-179 Poznań, Poland

E-mail: rj@wchuwr.chem.uni.wroc.pl

Received 17 February 2005, in final form 17 February 2005
Published 1 April 2005
Online at stacks.iop.org/JPhysCM/17/2509

Abstract

The crystal structures of $[C(NH_2)_3]_3[Sb_2Br_9]$ ($Gu_3Sb_2Br_9$) at 300 K and of $[C(NH_2)_3]_3[Sb_2Cl_9]$ ($Gu_3Sb_2Cl_9$) at 90 and 300 K are determined. The compounds crystallize in the monoclinic space group: $C2/c$. The structure is composed of $Sb_2X_9^{3-}$ (X = Cl, Br) ions, which form two-dimensional layers through the crystal, and guanidinium cations. In $Gu_3Sb_2Br_9$ the structural phase transformation of the first-order type is detected at 435/450 K (on cooling/heating) by the DSC and dilatometric techniques. The dielectric relaxation process in the frequency range between 75 kHz and 5 MHz over the low temperature phase indicates reorientations of weakly distorted guanidinium cations. The proton ^{1}H NMR second-moment and spin–lattice relaxation time, T_1, temperature runs for the polycrystalline $Gu_3Sb_2Br_9$ sample indicate a complex cation motion. A significant dynamical non-equivalence of two guanidinium cations was found. The possible mechanism of the phase transition in $Gu_3Sb_2Br_9$ is discussed on the basis of the results presented.

1. Introduction

The family of halogenoantimonates(III) and halogenobismuthates(III) of the general formula $R_aM_bX_{(3b+a)}$ (where R denotes the organic cation, M denotes metal Sb(III) or Bi(III) and X denotes a halogen atom, Cl, Br, I) is a promising group of materials from the point of view of non-linear dielectric properties. Among these molecular–ionic salts several ferroelectrics have been discovered. The majority of the ferroelectric salts crystallize with the $R_3M_2X_9$ [1–6] or $R_5M_2X_{11}$ [7–10] composition. Four forms of the anionic sublattice may be distinguished

[4] Author to whom any correspondence should be addressed.

in the group of the $R_3M_2X_9$ salts: (i) two-dimensional layer structure, (ii) infinite one-dimensional chains, (iii) discrete bioctahedral units and (iv) tetraoctahedral units [3]. In all structures three out of six halogen atoms in the octahedral unit, MX_6, are terminal and the other three are bridging. The ferroelectric properties were found only for salts characterized by the two-dimensional anionic sublattice. The anionic sublattice of the other subclass of the halogenoantimonates(III) and halogenobismuthates(III), $R_5Bi_2X_{11}$, is exclusively built up of discrete bioctahedral units, $Bi_2X_{11}^{5-}$. All salts, crystallizing with this stoichiometry possess ferroelectric properties. The origin of the ferroelectricity of either $R_3M_2X_9$ or $R_5Bi_2X_{11}$ subclass is ascribed to the dynamical disorder of dipolar organic cations as well as to the large polarizability of the anionic sublattice.

Recently, a ferroelectric crystal belonging to the chloroantimonate(III) salts, namely (4-NH_2PyH)$SbCl_4$, built up of polymeric anionic chains and the substituted pyridinium cations, has been found [11]. It reveals the ferroelectric phase transition at 271 K with the mechanism clearly of a displacive type. This is in contrast to an order–disorder mechanism of the structural phase transformation disclosed in the majority ferroelectrics described above. The phase situation in (4-NH_2PyH)$SbCl_4$ is rather complex since it discloses the incommensurate modulated intermediate phases.

The guanidinium antimonate(III) derivatives were found to crystallize with either $Gu_3Sb_2Cl_9$ or $Gu_3Sb_2Cl_5$·GuCl composition. Both chlorine salts revealed an interesting sequence of phase transitions connected with the dynamics of guanidinium cations. In this paper the results of studies on the synthesis and thermal properties, dilatometric and differential scanning calorimetry (DSC) of the bromide salts, $Gu_3Sb_2Br_9$, are described. Moreover the crystal structure at 300 K and the results of dielectric dispersion and proton magnetic resonance studies (^{1}H NMR) are presented. A possible mechanism of the phase transitions in the $Gu_3Sb_2Br_9$ crystals is discussed. The structural properties of the $Gu_3Sb_2Cl_9$ and $Gu_3Sb_2Br_9$ analogues are compared.

2. Experimental details

Crystals of the title compound were grown by a slow evaporation of a concentrated HBr solution containing a 3:4 ratio of $[C(NH_2)_3]_2CO_3$ and $SbBr_3$. The salts obtained were twice recrystallized and characterized by an elemental analysis. The single crystals were grown from an aqueous solution at constant room temperature. Differential scanning calorimetry (DSC) runs were recorded using a Perkin-Elmer DSC-7 in the temperature range 100–470 K. The TGA measurements were performed on a Setaram SETSYS 16/18 instrument in the temperature range 300–500 K with a ramp rate 2 K min^{-1}. The scan was performed in flowing nitrogen (flow rate: 1 dm^3 h^{-1}). The dilatometric measurements were performed by a thermomechanical analyser, Perkin-Elmer TMA-7, in the temperature range 140–300 K. The dimensions of the sample were of the order of $5 \times 3 \times 1$ mm^3.

The complex dielectric permittivity $\epsilon^* = \epsilon' - i\epsilon''$ was measured using HP 4285A and Agilent 4284A Precision LCR Meters in the frequency range between 1 kHz and 25 MHz and in the temperature range from 100 to 460 K. The dimensions of the sample were of the order of $5 \times 3 \times 1$ mm^3. The overall errors in estimation of the real and imaginary parts of the complex dielectric permittivity value were less than 5% and 10%, respectively.

NMR measurements were carried out with a Bruker SXP 4-100 spectrometer working at the frequency of 24.7 and 90 MHz. The standard Bruker temperature system (90 MHz) has been applied for automatical stabilization of the temperature of a sample from the liquid nitrogen temperature up to 487 K. In a Leybold temperature controller (24.7 MHz) the liquid helium was used as a cooling medium from 50 K up to the room temperature. The relaxation

times, T_1, were determined by using the $\pi-\tau-\pi/2$ sequence of pulses for times shorter than 1 s. For longer times the saturation method was used. The measurements of the proton NMR second moment were carried out with a wide-line spectrometer operating at 25 MHz. The second moments were calculated by numeral integration of the first derivative of an absorption line and corrected for the finite modulation amplitude. The powdered sample were degassed under pressure of 10^{-5} Torr and sealed in glass ampoules.

Single crystals of $Gu_3Sb_2Cl_9$ of dimensions $0.3 \times 0.3 \times 0.25$ mm^3 and $Gu_3Sb_2Br_9$ of $0.12 \times 0.2 \times 0.25$ mm^3 were selected for the x-ray diffraction studies. Measurements on $Gu_3Sb_2Cl_9$ were made using a KUMA KM-4 diffractometer, while those on $Gu_3Sb_2Br_9$ were made with an Oxford Diffraction CCD κ-axis diffractometer with graphite monochromated Mo Kα ($\lambda = 0.71073$ Å) radiation. For $Gu_3Sb_2Cl_9$ two data sets were collected, one at ambient temperature, the other at 90.0(1) K. The low temperature was stabilized using an Oxford Cryosystem open flow cooler. The temperature stability was of the order of ± 0.1 K.

For $Gu_3Sb_2Br_9$ the unit cell parameters were obtained from the least squares refinement of 30 reflections in the 2Θ range 12°–26°. A total of 2016–2186 reflections were measured in the 2Θ range $6° \leqslant 2\Theta \leqslant 50°$ using the ω–Θ scan technique. Two standard reflections monitored every 50 showed that the intensity variation was negligible. Lorentz, polarization and semi-empirical absorption corrections (via ψ-scans, based on reflection measurements at different azimuthal angles [12]) were applied ($T_{min} = 0.20$, $T_{max} = 0.37$).

The $Gu_3Sb_2Br_9$ crystal was positioned at 65 mm from the KM4CCD camera and 612 frames were measured at 0.75° intervals with a counting time of 20 s. The data were corrected for Lorentz and polarization effects. Analytical absorption correction was also applied. Data collections, integration and scaling of the reflections and analytical absorption correction were carried out using the CrysAlis suite of programs [12]. The two crystals appear to be isomorphic at room temperature. From systematic absences, monoclinic Cc and $C2/c$ space groups follow. On the basis of the statistics of normalized structure factors $E(E-1) = 1.053$ (0.918 theoretically for centrosymmetric and 0.736 for non-centrosymmetric space groups), the centrosymmetric $C2/c$ space group was selected. The structure was solved by the Patterson method (Sb, Cl or Br atoms) and refined by a full-matrix least squares method. All other atoms were located from difference Fourier synthesis. All hydrogen atoms were included using standard geometric criteria. Hydrogen atoms of NH_2 were constrained to the distance of 0.90 Å. KUMA software was used in the data collection, cell refinement and data reduction processes [12]. The SHELX-97 [14] program was used for the structure solution and refinement. The structure drawings were prepared using the SHELXTL program [15].

Crystallographic data for the structures reported in this paper have been deposited with the Cambridge Crystallographic Data Centre, CCDC No CCDC 257220-257222. Copies of this information may be obtained free of charge from the Director, CCDC, 12 Union Road, Cambridge CB2 1EZ, UK (fax: +44-1223-336033; e-mail: deposit@ccdc.cam.ac.uk or http://www.ccdc.cam.ac.uk).

3. Results

3.1. X-ray studies

The redetermination of the crystal structure of $Gu_3Sb_2Cl_9$ proved that the previous solution [16] was not correct. The difference between the present and previous positions of atoms is a shift of all atomic coordinates in the present solution to $(x - 0.5, 1.5 - y, z)$. Placement of atoms in incorrect positions resulted in the presence of Fourier peaks interpreted, erroneously, as disordered water molecules. Except for spurious water molecules, all other data remain as

Table 1. Crystal data and structure refinement for $[C(NH_2)_3]_3[Sb_2X_9]$ (X = Cl, Br).

Empirical formula	$[C(NH_2)_3]_3[Sb_2Cl_9]$	$[C(NH_2)_3]_3[Sb_2Cl_9]$	$[C(NH_2)_3]_3[Sb_2Br_9]$
Formula weight	742.81	742.81	1142.95
Temperature (K)	300(2)	90(1)	300(2)
Wavelength (Å)		0.710 73	
Crystal system		Monoclinic	
Space group	$C2/c$	$C2/c$	$C2/c$
Unit cell dimensions (Å, deg)	$a = 15.244(3)$	15.161(3)	15.725(3)
	$b = 8.779(2)$	8.756(2)	9.040(2)
	$c = 17.882(3)$	17.428(3)	18.681(4)
	$\beta = 96.31(3)$	96.64(3)	96.68(3)
Volume ($Å^3$)	2378.6(8)	2298.0(8)	2637.6(10)
Z		4	
Calculated density (g cm^{-3})	2.074	2.147	2.878
Absorption coefficient (mm^{-1})	3.290	3.405	15.691
$F(000)$		1416	2064
Theta range for data collection (deg)	3–25	3–25	3–30
Index ranges	$-18 \Leftarrow h \Leftarrow 0$	$-18 \Leftarrow h \Leftarrow 0$	$-21 \Leftarrow h \Leftarrow 19$
	$-10 \Leftarrow k \Leftarrow 0$	$-9 \Leftarrow k \Leftarrow 0$	$-12 \Leftarrow k \Leftarrow 12$
	$-21 \Leftarrow l \Leftarrow 21$	$-20 \Leftarrow l \Leftarrow 20$	$-25 \Leftarrow l \Leftarrow 24$
Reflections collected/unique	2186/2103	2094/2016	9327/3447
R_{int}	0.017	0.032	0.0611
Refinement method		Full-matrix least squares on F2	
Data/restraints/parameters	2103/0/125	2016/0/125	3447/0/124
Goodness-of-fit on F^2	1.283	1.339	0.878
Final R indices ($I > 2\sigma(I)$)	$R_1 = 0.0255$	0.0298	0.0454
	$wR_2 = 0.0738$	0.0818	0.0962
R indices (all data)	$R_1 = 0.0285$	0.0311	0.0920
	$wR_2 = 0.0751$	0.0827	0.1073
Extinction coefficient	0.0041(2)	0.0004(1)	—
Largest diff. peak/hole (e $Å^{-3}$)	0.666/−0.467	1.146/−0.979	0.982/−1.024

previously determined. Crystallographic data and details on the structure determinations of $Gu_3Sb_2X_9$ (X = Cl, Br) are given in table 1. The atomic coordinates and equivalent isotropic displacement parameters are presented in table 2. The two crystals are isomorphous, with monoclinic space group $C2/c$. The anionic sublattice of $Gu_3Sb_2X_9$ is presented as plots seen in two perpendicular directions in figure 1, whereas in figure 2 we show the molecular structure of $Gu_3Sb_2Br_9$. The sublattice is composed of distorted SbX_6^{3-} octahedra, connected with each other by bridging halogen atoms, forming a honeycomb structure. The independent antimony atoms lie at the centre of a distorted octahedral unit. The X–Sb–X bond angles are within 84.90(4)° and 97.65(4)° at 300 K and 84.69(4)° and 98.24(4)° at 90 K for $Gu_3Sb_2Cl_9$ and between 85.55(3)° and 95.51(3)° for $Gu_3Sb_2Br_9$ at 300 K (table 3). The anionic octahedra are, therefore, more distorted and low temperature leads to an increasing of the distortion. The Sb–X bond lengths fall into two ranges. For $Gu_3Sb_2Cl_9$ at 90.0(1) K they are between 2.466(1) and 2.925(1) Å and for $Gu_3Sb_2Br_9$ between 2.607(1) and 3.087(1) Å. The longer bonds are characteristic for bridging halogen atoms and the shorter ones correspond to the terminal halogens. The difference between the longest and shortest Sb–X bonds is not large. It is 0.459(1) Å for chlorine and 0.480(1) Å for bromine analogues. Generally analogous bromine bonds are 0.14 Å longer in comparison to the chlorine ones.

There are two independent guanidinium cations in the structure. One, disordered (C(2)), is located in voids of the polyanionic sublattice (figure 2); the other one (C(1)), ordered, is

Table 2. Atomic coordinates ($\times 10^4$) and equivalent isotropic displacement parameters ($Å^2 \times 10^3$) for $Gu_3Sb_2X_9$ (X = Cl, Br). U_{eq} is defined as one third of the trace of the orthogonalized U_{ij} tensor.

	x	y	z	U_{eq}
		$Gu_3Sb_2Cl_9$ at 300 K		
Sb(1)	1555(1)	4 012(1)	1664(1)	35(1)
Cl(1)	802(1)	6 032(1)	900(1)	48(1)
Cl(2)	2786(1)	4 035(1)	894(1)	48(1)
Cl(3)	811(1)	2 096(1)	831(1)	55(1)
Cl(4)	2493(1)	1 495(1)	2503(1)	52(1)
Cl(5)	0	3 967(2)	2500	52(1)
C(1)	1869(3)	5 953(5)	−871(2)	45(1)
N(1)	1440(3)	4 668(4)	−836(2)	54(1)
N(2)	1436(3)	7 245(5)	−883(2)	62(1)
N(3)	2722(3)	5 955(5)	−883(3)	62(1)
C(2)	33(12)	8 978(9)	2675(5)	45(3)
N(4)	−827(5)	8 995(10)	2673(6)	67(2)
N(5)	444(5)	10 264(10)	2673(6)	70(2)
N(6)	459(5)	7 706(9)	2713(5)	61(2)
		$Gu_3Sb_2Cl_9$ at 90 K		
Sb(1)	1554(1)	4 001(1)	1662(1)	16(1)
Cl(1)	791(1)	6 025(1)	876(1)	19(1)
Cl(2)	2787(1)	4 020(1)	874(1)	19(1)
Cl(3)	798(1)	2 070(1)	810(1)	21(1)
Cl(4)	2493(1)	1 486(1)	2505(1)	21(1)
Cl(5)	0	3 959(2)	2500	21(1)
C(1)	1872(3)	5 974(5)	−877(3)	19(1)
N(1)	1439(3)	4 663(5)	−859(2)	21(1)
N(2)	1441(3)	7 278(5)	−882(2)	23(1)
N(3)	2745(3)	5 976(5)	−878(2)	23(1)
C(2)	34(9)	8 970(11)	2695(4)	19(2)
N(4)	−842(5)	8 982(10)	2704(5)	23(2)
N(5)	453(5)	10 271(10)	2692(5)	26(2)
N(6)	457(5)	7 669(10)	2723(5)	23(2)
		$Gu_3Sb_2Br_9$ at 300 K		
Sb(1)	1544(1)	3 955(1)	1623(1)	35(1)
Br(1)	757(1)	6 066(1)	860(1)	48(1)
Br(2)	2829(1)	3 983(1)	855(1)	47(1)
Br(3)	763(1)	1 949(1)	782(1)	54(1)
Br(4)	2493(1)	1 431(1)	2496(1)	50(1)
Br(5)	0	3 905(1)	2500	50(1)
C(1)	1874(5)	6 030(9)	−885(4)	42(2)
N(1)	1468(4)	4 761(8)	−845(4)	61(2)
N(2)	1460(4)	7 259(8)	−901(4)	63(2)
N(3)	2714(4)	6 018(8)	−894(4)	66(2)
C(2)	60(2)	8 931(16)	2686(10)	43(6)
N(4)	−802(8)	8 973(19)	2687(9)	72(5)
N(5)	447(9)	10 167(17)	2675(10)	76(5)
N(6)	450(9)	7 660(16)	2718(9)	67(4)

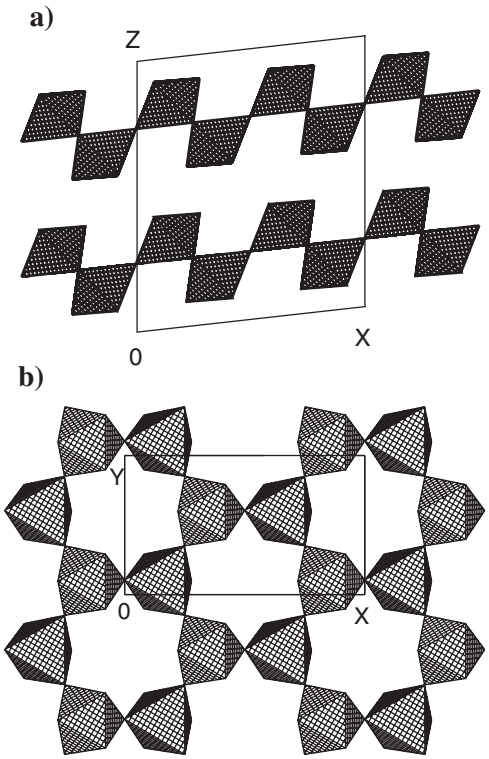

Figure 1. Anionic structure as a polyhedral representation along (a) the ***b***-axis and (b) ***c***-axis.

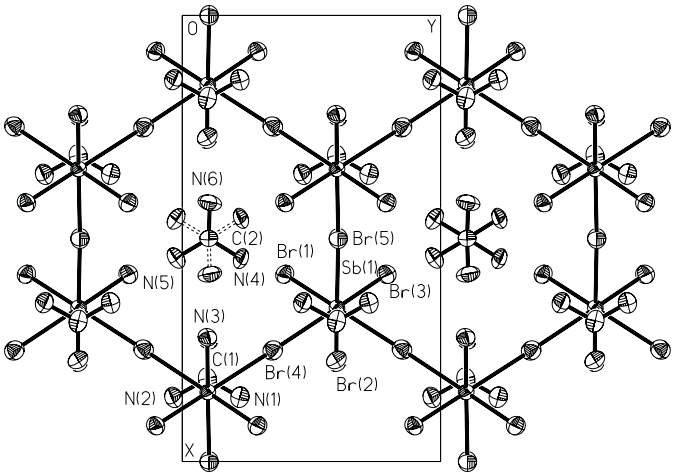

Figure 2. Crystal packing down the ***c***-axis in $Gu_3Sb_2Br_9$.

placed between the anionic layers. The disorder of the cation is realized by the presence of two positions of all C, N and H atoms. Two positions are generated by rotation of the molecule around the axis perpendicular to the CN_3 plane in 60° steps. Initially we placed the C(2) atom on the inversion centre. It resulted (especially at 90 K) in a much elongated thermal displacement ellipsoid of the C(2) atom in the direction perpendicular to the CN_3

Table 3. Bond lengths (Å) and angles (deg) for $Gu_3Sb_2X_9$ (X = Cl, Br).

	300 K X = Cl	90 K X = Cl	300 K X = Br
Sb(1)–Cl(1)	2.446(1)	2.447(1)	2.607(1)
Sb(1)–Cl(2)	2.447(1)	2.446(1)	2.611(1)
Sb(1)–Cl(3)	2.442(1)	2.446(1)	2.612(1)
Sb(1)–Cl(4)	2.950(1)	2.925(1)	3.087(1)
Sb(1)–Cl(4)#1	2.934(1)	2.905(1)	3.071(1)
Sb(1)–Cl(5)	2.939(1)	2.911(1)	3.083(1)
C(1)–N(1)	1.308(5)	1.325(6)	1.319(9)
C(1)–N(2)	1.311(6)	1.315(6)	1.286(9)
C(1)–N(3)	1.303(5)	1.323(6)	1.324(9)
C(2)–N(4)	1.310(14)	1.329(13)	1.35(2)
C(2)–N(5)	1.292(14)	1.305(13)	1.27(2)
C(2)–N(6)	1.291(13)	1.306(13)	1.30(2)
Cl(1)–Sb(1)–Cl(2)	91.25(4)	91.29(4)	92.34(2)
Cl(1)–Sb(1)–Cl(3)	90.06(5)	90.17(5)	91.08(4)
Cl(1)–Sb(1)–Cl(4)	176.63(4)	176.09(4)	178.73(3)
Cl(1)–Sb(1)–Cl(4)#1	84.98(4)	85.01(4)	86.15(4)
Cl(1)–Sb(1)–Cl(5)	86.49(4)	86.16(4)	87.01(3)
Cl(2)–Sb(1)–Cl(3)	89.81(4)	89.89(4)	90.89(3)
Cl(2)–Sb(1)–Cl(4)	86.18(4)	85.83(4)	86.59(3)
Cl(2)–Sb(1)–Cl(4)#1	84.90(4)	84.69(4)	85.55(3)
Cl(2)–Sb(1)–Cl(5)	176.38(3)	175.92(3)	178.72(3)
Cl(3)–Sb(1)–Cl(4)	87.74(4)	87.17(4)	88.24(4)
Cl(3)–Sb(1)–Cl(4)#1	173.04(4)	172.65(4)	175.40(3)
Cl(3)–Sb(1)–Cl(5)	87.36(4)	86.94(4)	88.01(3)
Cl(4)–Sb(1)–Cl(4)#1	96.49(2)	97.35(2)	94.46(3)
Cl(5)–Sb(1)–Cl(4)#1	97.65(3)	98.24(4)	95.51(3)
Cl(4)–Sb(1)–Cl(5)	95.96(3)	96.56(4)	94.04(3)
Sb(1)#2–Cl(4)–Sb(1)	179.31(4)	179.34(5)	179.11(3)
Sb(1)–Cl(5)–Sb(1)#3	178.45(6)	178.55(6)	178.31(5)
N(1)–C(1)–N(2)	119.5(4)	120.3(4)	120.4(8)
N(1)–C(1)–N(3)	120.4(4)	119.9(4)	119.0(8)
N(2)–C(1)–N(3)	120.0(4)	119.7(4)	120.6(8)
N(4)–C(2)–N(5)	118.4(15)	118.7(11)	117(3)
N(4)–C(2)–N(6)	120.5(15)	119.6(11)	120(3)
N(5)–C(2)–N(6)	121.0(15)	121.6(11)	123(3)

Symmetry transformations used to generate equivalent atoms:
#1 $-x+1/2, y+1/2, -z+1/2$ #2 $-x+1/2, y-1/2, -z+1/2$ #3 $-x, y, -z+1/2$

plane. We decided to move the carbon atom out of the symmetry centre. This resulted in planar arrangement of carbon and nitrogen atoms and much less distorted C–N bond lengths and angles. The symmetry planes of those two disordered molecules are about 0.68 Å apart. The guanidinium cations are bounded to the anionic sublattice by weak N–H $\cdots$ X hydrogen bonds. The shortest N–H $\cdots$ X hydrogen contacts are listed in table 4.

In $Gu_3Sb_2X_9$ hydrogen bonds have H $\cdots$ Cl distances of 2.49–2.60 Å (at 300 K) and 2.48–2.58 Å (at 90.0(1) K), whereas those for H $\cdots$ Br are in the range 2.62–2.70 Å. The N $\cdots$ Cl distances are between 3.327(8) and 3.384(4) Å (at 300 K) and between 3.310(8) and 3.459(4) Å (at 90.0(1) K). The N $\cdots$ Br distances are in the 3.451(15)–3.601(7) Å range. The N(1) cation, placed between the polyanionic layers, shows significantly longer N $\cdots$ Cl

Table 4. Hydrogen bonds for Gu_3Sb_2X (X = Cl, Br) (Å) and angles (deg).

D–H···A	*d* (D–H)	*d*(H···A)	*d*(D···A)	<(DHA)
		$Gu_3Sb_2Cl_9$ at 300 K		
N(1)–H(1A)···Cl(2)#4	0.90	2.58	3.464(4)	166
N(1)–H(1B)···Cl(1)#5	0.90	2.58	3.462(4)	165
N(2)–H(2A)···Cl(2)#6	0.90	2.59	3.476(4)	167
N(2)–H(2B)···Cl(3)#5	0.90	2.60	3.484(4)	167
N(3)–H(3A)···Cl(1)#6	0.90	2.60	3.475(4)	166
N(3)–H(3B)···Cl(3)#4	0.90	2.60	3.484(4)	167
N(4)–H(4A)···Cl(4)#7	0.90	2.54	3.362(8)	152
N(4)–H(4B)···Cl(4)#8	0.90	2.51	3.344(8)	155
N(5)–H(5A)···Cl(4)#9	0.90	2.53	3.350(8)	152
N(5)–H(5B)···Cl(5)#9	0.90	2.49	3.327(8)	155
N(6)–H(6A)···Cl(5)	0.90	2.56	3.369(8)	150
N(6)–H(6B)···Cl(4)#1	0.90	2.52	3.360(8)	155
		$Gu_3Sb_2Cl_9$ at 90 K		
N(1)–H(1A)···Cl(2)#4	0.90	2.55	3.432(4)	167
N(1)–H(1B)···Cl(1)#5	0.90	2.55	3.432(4)	166
N(2)–H(2A)···Cl(2)#6	0.90	2.57	3.446(4)	166
N(2)–H(2B)···Cl(3)#5	0.90	2.58	3.459(4)	167
N(3)–H(3A)···Cl(1)#6	0.90	2.56	3.438(4)	166
N(3)–H(3B)···Cl(3)#4	0.90	2.57	3.456(4)	167
N(4)–H(4A)···Cl(4)#7	0.90	2.51	3.327(8)	152
N(4)–H(4B)···Cl(4)#8	0.90	2.48	3.316(8)	155
N(5)–H(5A)···Cl(4)#9	0.90	2.50	3.322(8)	152
N(5)–H(5B)···Cl(5)#9	0.90	2.48	3.310(8)	155
N(6)–H(6A)···Cl(5)	0.90	2.52	3.334(9)	150
N(6)–H(6B)···Cl(4)#1	0.90	2.50	3.342(8)	156
		$Gu_3Sb_2Br_9$ at 300 K		
N(1)–H(1B)···Br(2)#4	0.90	2.69	3.562(7)	163
N(1)–H(1A)···Br(1)#5	0.90	2.70	3.574(6)	164
N(2)–H(2B)···Br(2)#6	0.90	2.70	3.574(7)	163
N(2)–H(2A)···Br(3)#5	0.90	2.73	3.601(7)	164
N(3)–H(3A)···Br(1)#6	0.90	2.69	3.564(6)	164
N(3)–H(3B)···Br(3)#4	0.90	2.71	3.585(7)	164
N(4)–H(4A)···Br(4)#7	0.90	2.70	3.518(15)	152
N(4)–H(4B)···Br(4)#8	0.90	2.62	3.451(15)	154
N(5)–H(5A)···Br(4)#9	0.90	2.65	3.466(8)	155
N(5)–H(5B)···Br(5)#9	0.90	2.62	3.459(8)	152
N(6)–H(6A)···Br(5)	0.90	2.67	3.482(15)	150
N(6)–H(6B)···Br(4)#1	0.90	2.65	3.488(14)	155

Symmetry transformations used to generate equivalent atoms:
#1 $-x+1/2, y+1/2, -z+1/2$ #2 $-x+1/2, y-1/2, -z+1/2$
#3 $-x, y, -z+1/2$ #4 $-x+1/2, -y+1/2, -z$ #5 $-x, -y+1, -z$
#6 $-x+1/2, -y+3/2, -z$ #7$x-1/2, y+1/2, z$ #8 $-x, y+1, -z+1/2$
#9 $x, y+1, z$

distances, which suggests that it is more loosely bound to the crystal lattice. One can state, however, that the hydrogen bonds in $Gu_3Sb_2X_9$ systems are quite weak, which may justify the disorder of the C(2) cation.

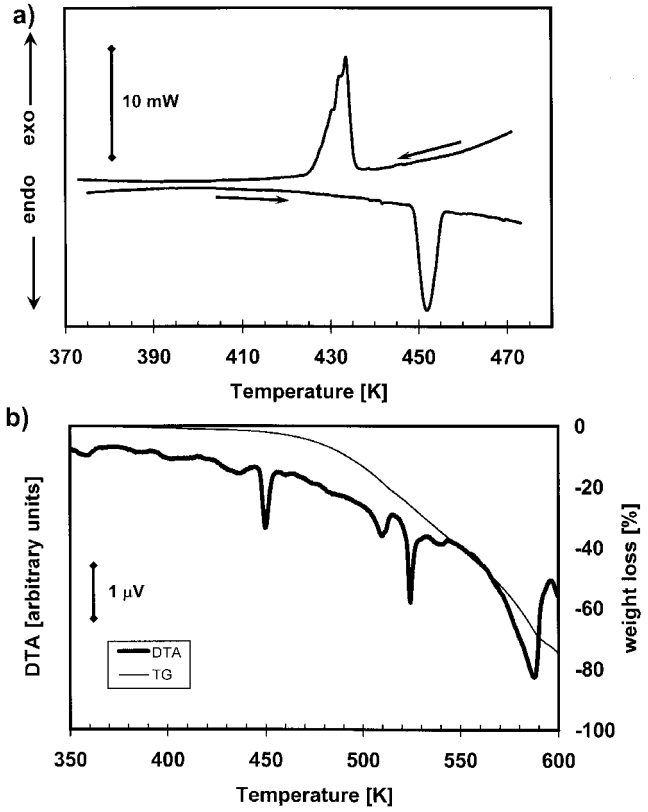

Figure 3. (a) DSC runs (on cooling and heating; DSC with the ramp rate of 10 K min^{-1}; sample mass: 14.062 mg) and (b) simultaneous thermogravimetric analysis (TGA) and differential thermal analysis (DTA) scans for the $Gu_3Sb_2Br_9$ crystals.

The determination of the crystal structure of $Gu_3Sb_2Cl_9$ at 90.0(1) K shows that its symmetry does not change from 300 to 90.0(1) K. The type of the disorder does not change with temperature either. This suggests that the observed disorder is statistical in nature. It does not exclude, however, the possibility of the rotational C_3 type of motion for both cations. Judging from shorter $N \cdots Cl$ distances, one should expect the C_3 rotation to be more hindered in the case of C(2) in comparison to C(1) cations.

3.2. Differential scanning calorimetry (DSC) and linear thermal expansion measurements

The results of the calorimetric and thermogravimetric analysis for $Gu_3Sb_2Br_9$ are illustrated in figure 3. The $Gu_3Sb_2Br_9$ crystals continuously lose about 3% of their mass approaching $T_m = 470$ K (see figure 3(b)). When the sample is heated from room temperature up to 470 K it reveals one reversible heat anomaly at 450/435 K—heating–cooling (see figure 3(a)). This anomaly exhibits all features typical of the first-order phase transition—a well shaped peak on the DSC curve and the temperature hysteresis. The value of the entropy effect, ΔS, is equal to 51 J mol^{-1} K^{-1}, which is rather high for such crystals. The high temperature phase is denoted as I whereas the low temperature phase, that below 435 K, is denoted as II.

Figure 4 shows the results on the linear thermal expansion, $\Delta L/L_0$, obtained along the $\boldsymbol{a}$-, $\boldsymbol{b}$- and $\boldsymbol{c}$-axes (the notation is according to the monoclinic system, phase II) for the $Gu_3Sb_2Br_9$

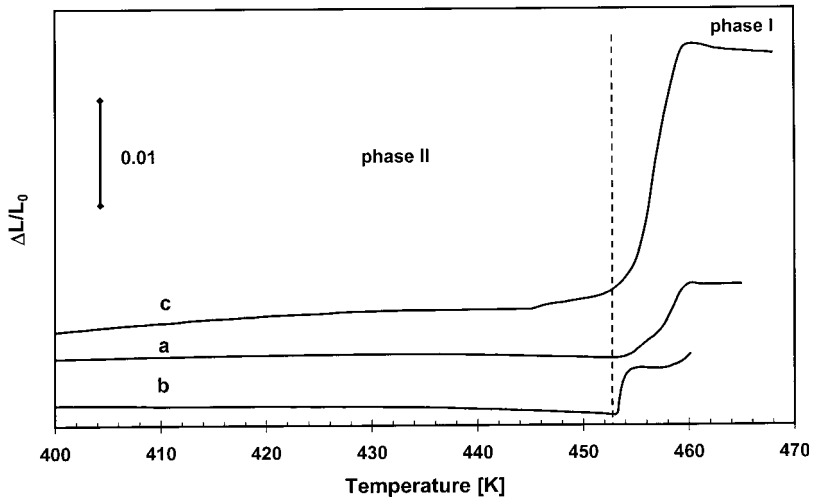

Figure 4. Temperature dependence of the linear thermal expansion, $\Delta L/L_0$, measured along the a-, b- and c-axes (monoclinic system, phase II) at a ramp rate 4 K min^{-1} for $Gu_3Sb_2Br_9$.

samples. We can state that dilatometric results are highly consistent with the data obtained in the DSC measurements. The transformation at 450 K, on heating, in $Gu_3Sb_2Br_9$ (figure 4) is accompanied by a $\Delta L/L_0$ change characteristic of a discontinuous transformation. That is, a stepwise change in the value of the linear thermal expansion, $\Delta L/L_0$, as large as $\sim 1 \times 10^{-2}$ and 2×10^{-2} parallel and perpendicular to the ab cleavage plane, respectively, is observed at the phase transformation temperature. The phase transformation at 450 K is accompanied by a rapid increase of the dimensions of the sample in all directions and causes a cracking of the crystal. This is one reason that the dilatometric scans are not perfectly reversible on cooling. Nevertheless the anomaly in $\Delta L/L_0$ corresponding to the phase transition is observed during the cooling scans as well (not shown in figure 4).

No anomaly in dilation of the crystal is observed when the crystal is cooled from room temperature down to 100 K.

On the basis of the DSC and dilatometric results the pressure coefficient, $\mathrm{d}T_C/\mathrm{d}p$, can be estimated according to the relationship

$$\frac{\mathrm{d}T_\mathrm{C}}{\mathrm{d}p} = \frac{\Delta V}{\Delta S} \tag{1}$$

where T_C is the temperature of the phase transformation, ΔV and ΔS are the changes of the molar volume and entropy at the transformation temperature, respectively. The pressure coefficient, $\mathrm{d}T_\mathrm{C}/\mathrm{d}p$, is equal to 0.23 K MPa^{-1}.

3.3. Dielectric relaxation studies

For $Gu_3Sb_2Br_9$ we performed measurements of the complex dielectric permittivity, ϵ^*, as a function of temperature and frequency. The purpose of these measurements was to determine the nature of the phase transition and to find the parameters of the presumably dielectric relaxation processes. The temperature dependence of the real and imaginary parts of the electric permittivity, $\epsilon' - \mathrm{i}\epsilon''$, along the c-axis (monoclinic system, phase II) for ten selected frequencies (between 300 kHz and 5 MHz) is presented in figures 5 and 6. Figure 5 shows the permittivity run in a temperature range where the clear dispersion of the real part of the electric

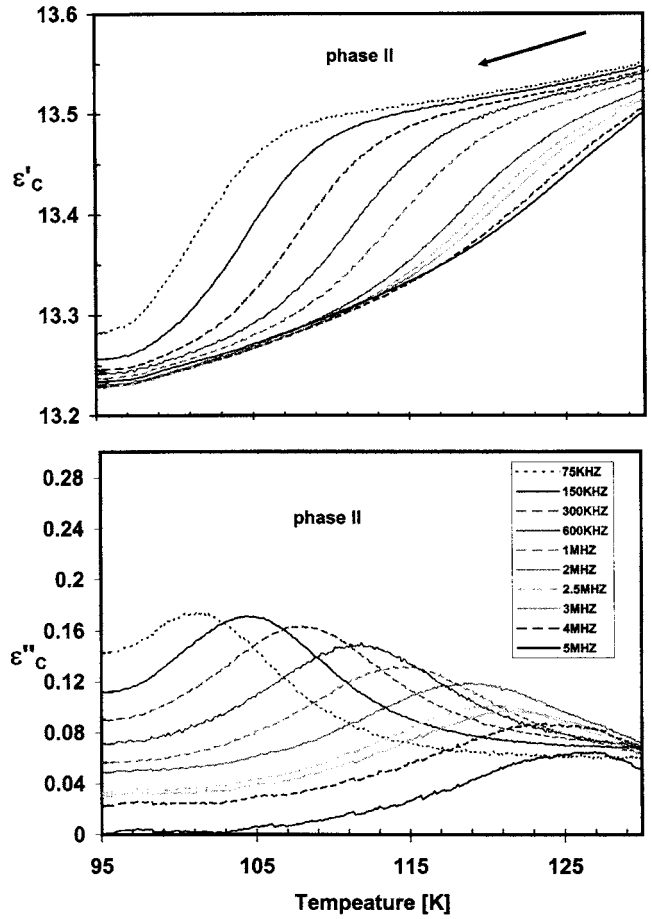

Figure 5. The temperature dependence of the real and imaginary parts of the complex electric permittivity, $\epsilon^* = \epsilon' - i\epsilon''$, for $Gu_3Sb_2Br_9$ along the *c*-axis for the selected frequencies in the low temperature region.

permittivity, ϵ'_c, is observed. The dispersion in ϵ'_c is accompanied by absorption curves, the maxima of which are shifted towards higher temperatures with frequency increasing. Figure 6 shows the dielectric response in the vicinity of the I $\rightarrow$ II phase transition detected by the DSC and dilatometric techniques. Over phase II a monotonic increase of ϵ'_c is observed. Above the II $\rightarrow$ I transformation the discrepancies in permittivity runs at various frequencies are caused, most probably, by the appearance of the electric conductivity, which is usually observed in halogenoantimonates(III) or halogenobismuthates(III) at high temperatures.

Since over the phase II a clear dispersion of the real part of the dielectric permittivity has been observed, we decided to perform a detailed study of the dielectric relaxation process. The Cole–Cole diagrams at several selected temperatures are presented in figure 7. It was found that the dielectric response in $Gu_3Sb_2Br_9$ crystals is well described by the Cole–Cole relationship [17]:

$$\epsilon^* = \epsilon_\infty + \frac{\epsilon_0 - \epsilon_\infty}{1 + (i\omega\tau)^{1-\alpha}} \tag{2}$$

where ϵ_0 and ϵ_∞ are the low and high frequency limits of the electric permittivity, respectively,

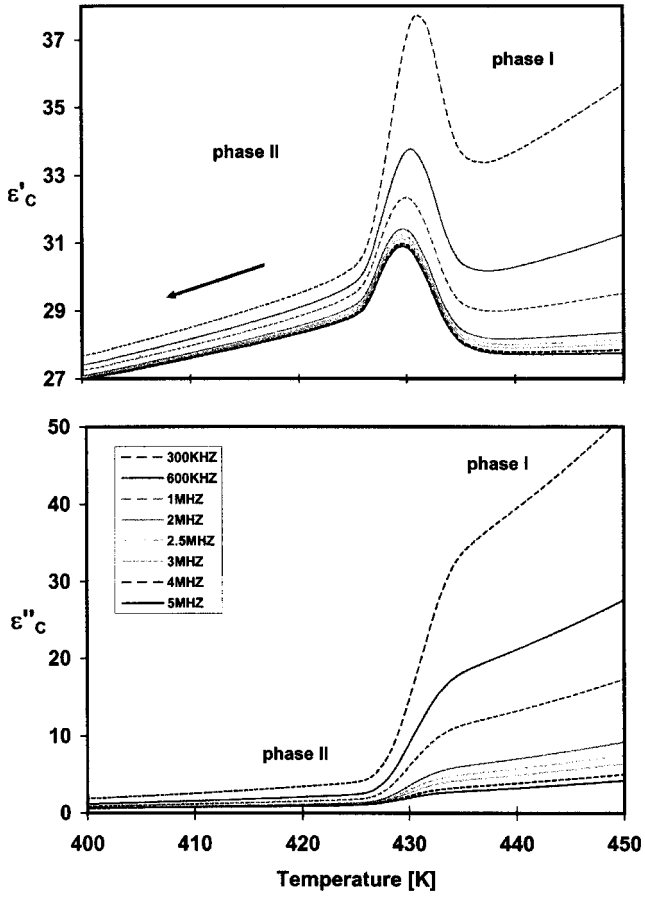

Figure 6. The temperature dependence of the real and imaginary parts of the complex electric permittivity, $\epsilon^* = \epsilon' - \mathrm{i}\epsilon''$, for $Gu_3Sb_2Br_9$ along the *c*-axis for the selected frequencies in the vicinity of the II–I phase transition temperature (on cooling).

ω is the angular frequency, τ is the mean relaxation time and α is the parameter of distribution of the relaxation times.

We have fitted the experimental Cole–Cole plots at several temperatures using equation (2) in order to estimate the relaxation parameters: $\epsilon_0, \epsilon_\infty, \alpha$ and τ. The parameters of the relaxation process are collected in table 5. An important increase in the macroscopic relaxation time τ (about one order of magnitude in the interval of 100–115 K) indicates a substantial slowing down of the relaxation process on cooling. The small value of the distribution parameter, α, equal to about 0.03 at 100 K, shows that the dielectric spectrum is almost monodispersive in the interval of temperature corresponding to the observed dielectric relaxation process. It should be noted that the value of ϵ_0 ($\sim$13.6) is almost temperature independent.

The energy barrier, E_a, for the dipolar reorientation was estimated from an Arrhenius-type relationship for the macroscopic relaxation time:

$$\tau = C \exp\left(\frac{E_a}{kT}\right). \tag{3}$$

The activation energy estimated for this process (see figure 8) is equal to 22.6 kJ mol^{-1} and is typical of such crystals [18, 19].

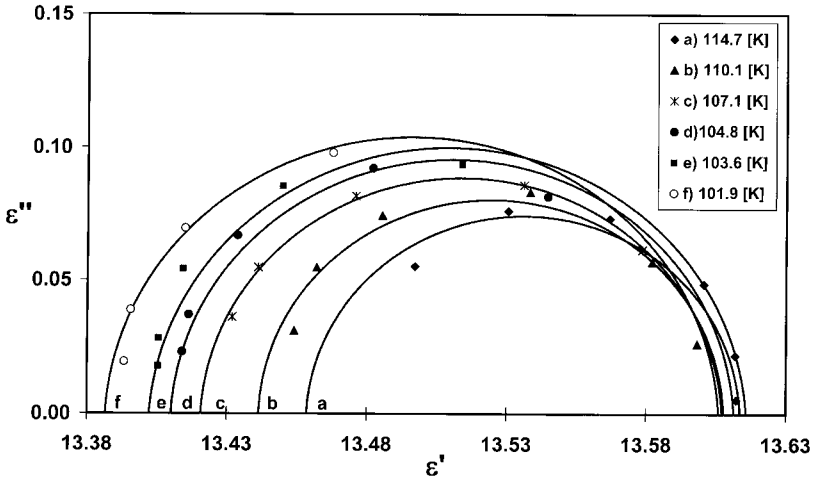

Figure 7. The Cole–Cole diagrams at the selected temperatures over phase II for $Gu_3Sb_2Br_9$.

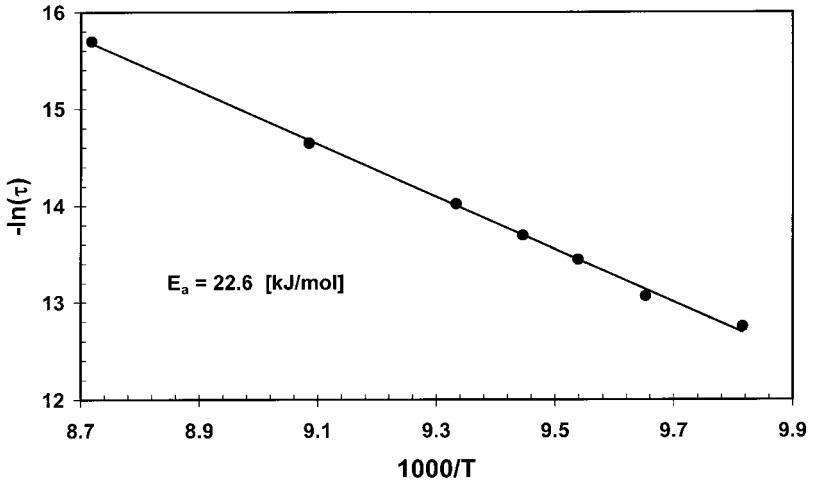

Figure 8. The Arrhenius-type plot for the dielectric macroscopic relaxation time, $\ln \tau$ versus $1/T$ for $Gu_3Sb_2Br_9$.

Table 5. Parameters of the relaxation process in $Gu_3Sb_2Br_9$.

T (K)	ϵ_0	ϵ_∞	τ (10^{-7} s)	α
101.9	13.606	13.387	28.9	0.035
103.6	13.616	13.402	21.2	0.042
104.8	13.611	13.41	14.47	0.034
107.1	13.607	13.421	8.1	0.033
110.1	13.608	13.441	4.34	0.022
114.7	13.614	13.459	1.52	0.027

3.4. MNR studies

3.4.1. Spin–lattice relaxation measurements. The dynamical non-equivalence of the guanidinium cations manifests itself in the existence of two or more T_1 minima of the T_1 versus

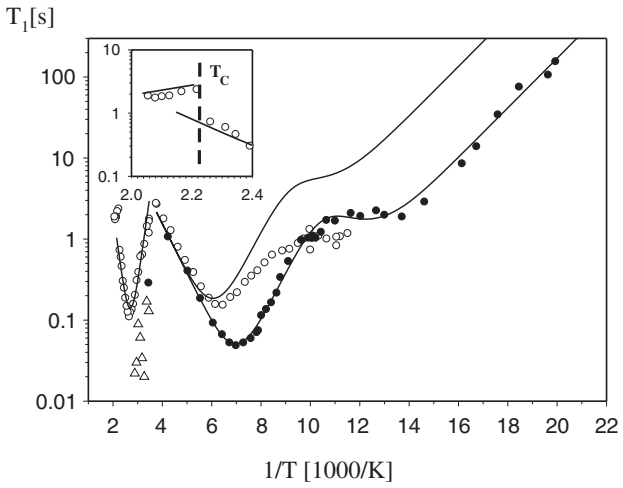

Figure 9. The temperature dependence of the spin–lattice relaxation times for protons at 90 MHz— ○—and at 24.7 MHz—●. △—the short component of the spin–lattice relaxation time T_1 at 90 MHz found only in the narrow temperature range. The solid line represents the results of the theoretical fit performed with the parameters from table 6.

$1/T$ curve. In the case of $Gu_3Sb_2Cl_9$ two T_1 minima have been ascribed to two different types of cation, each of them performing the C_3 type of motion [20]. The present x-ray studies show that the $Gu_3Sb_2Br_9$ crystals are characterized by two crystallography non-equivalent guanidinium cations as well. At room temperature cations of one kind (II), localized in a cavity formed by the polyanions, are disordered and cations of the other kind (I), localized between the polyanionic layers, are ordered. Moreover, the T_1 minimum at 372 K (90 MHz) is deeper than that at 153 K (90 MHz), which allows us to conclude that this minimum reflects the dynamics of two cations (type I) and the subsequent T_1 minimum is the result of the dynamics of the remaining one (type II); see figure 9. When the 24.7 MHz NMR spectrometer is used the third spin–lattice relaxation minimum appears at 82 K. This unexpected minimum cannot be explained in terms of a simple C_3 reorientation of all of the guanidinium cations. We decided to apply the same explanation of the guanidinium cationic dynamics as in the case of $[2\text{-}NH_2C_5H_4NH][SbBr_4]$ or $[2\text{-}NH_2C_5H_4NH][SbCl_4]$ [32]. That is, it was shown that the 2-aminopyridinium cation performs the pseudo-C_6 reorientations described by a non-equivalent well potential. According to the Ito *et al* model [21] an assumption is made that the guanidinium cation is performing C_6 reorientations about an axis which is perpendicular to the cationic plane. Since the guanidinium cation is planar and possesses six protons arranged in nearly sixfold symmetry this may be treated as an analogy to the pyridinium cation. The main reason for a choice of the Ito model was the presence of the characteristic double-minimum shape of the T_1 temperature dependence. The molecular dynamics for the system is described by the following expression, in which two relaxation contributions were taken into account:

$$\frac{1}{T_1} = C\left[\frac{3a}{(1+2a)^2} f(\tau_{c1}) + \frac{a}{(1+2a)} f(\tau_{c2})\right] \tag{4}$$

where

$$f(\tau_{ci}) = \frac{\tau_{ci}}{1+\omega_H^2\tau_{ci}^2} + \frac{4\tau_{ci}}{1+4\omega_H^2\tau_{ci}^2}. \tag{5}$$

Table 6. Dynamical parameters obtained from T_1 relaxation experiments for $Gu_3Sb_2Br_9$.

	Cation type	Motion mode	Activation energy (kJ mol^{-1})	Correlation time (s)	Relaxation constant (s^{-2})
	I	C_3	42	1.1×10^{-15}	3.2×10^9
Phase II			$E_A = 3.4$		
	II	C_6'	$E_B = 2.6$	2.2×10^{-13}	6.4×10^9
			$E_C = 1.4$		
Phase I	I + II	Isotropic rotation	4.7		

C is a relaxation constant. The correlation times τ_{c1} and τ_{c2} are defined by $\tau_{c1} = (2W_1 + W_2)^{-1}$ and $\tau_{c2} = (W_2 + 2W_3)^{-1}$ where W_1, W_2 and W_3 are the probability rates of the transition in the three-well potential. The probability rates for the transition of the cation between two different wells are defined by $W_1 = K\exp(-E_A/RT)$, $W_2 = K\exp(-E_B/RT)$ and $W_3 = K\exp(-E_C/RT)$, where K is a jumping frequency factor independent of temperature. The population parameter is given by $a = \exp[(E_B - E_A)/RT]$, where E_A, E_B and E_C are the activation energies, which characterize the three-well potential (see figure 11). As a result, the total rate $1/T_1$ over the whole temperature range studied is composed of two parts, the first one originating from the C_3 reorientation of the guanidinium cation of type I and the second one originating from complex pseudo-C_6 reorientation of the type II cations. The cations of type I and II occur in a 2:1 proportion—taking only the mutual number of cations instead of the number of protons:

$$\frac{1}{T_1} = \frac{2}{3}\left(\frac{1}{T_1}\right)^{\mathrm{I}}_{C3} + \frac{1}{3}\left(\frac{1}{T_1}\right)^{\mathrm{II}}_{C_6'}. \tag{6}$$

It should be noted that a third of the guanidinium cations show the complex pseudo-C_6-type motion modes at low temperatures but two thirds of them experience only the C_3 reorientation at high temperatures. This model of the dynamics of cations is also supported by x-ray experiment results as was mentioned above. The theoretical solid line for 24.7 MHz in figure 9 is the result of fitting the experimental points. The calculations permit us to obtain the dynamical parameters for relaxation of both kinds of cations (table 6).

Below 155 K, i.e. just below the minimum of the relaxation time, T_1 (90 MHz), there are observed some irregularities with respect to the known quadratic dependence of the Larmor frequency in the temperature dependences of the relaxation time. We interpret this as a result of the cross-relaxation phenomenon of proton spins and quadrupole nucleus spins, similar to the observed irregular dynamics of the pyridinium cation in $(C_5H_5NH)_5Bi_2Br_{11}$ [22]. But due to the limitations of the cooling system working at 90 MHz (only a liquid nitrogen cooler is allowed) we were not able to lower the temperature.

Above 451 K a sudden change in the character of the temperature dependence of the relaxation time is observed (see the inset in figure 9). Over the high temperature phase (I) the relaxation time decreases on heating with the activation energy equal to 19.7 kJ mol^{-1}, which is almost twice as small as that in the low temperature phase (II).

3.4.2. The second-moment measurements. Results of the analysis of the second-moment values for protons, M_2, in figure 10 show that between 94 and 122 K the value of M_2 is continuously reduced from 18.5 G^2 to about 14 G^2 and no plateau at low temperatures is observed. Between 122 and 224 K, a plateau at the value 14 G^2 is observed and then M_2 decreases abruptly to 2.5 G^2. Above 275 up to 349 K the second-moment value is maintained

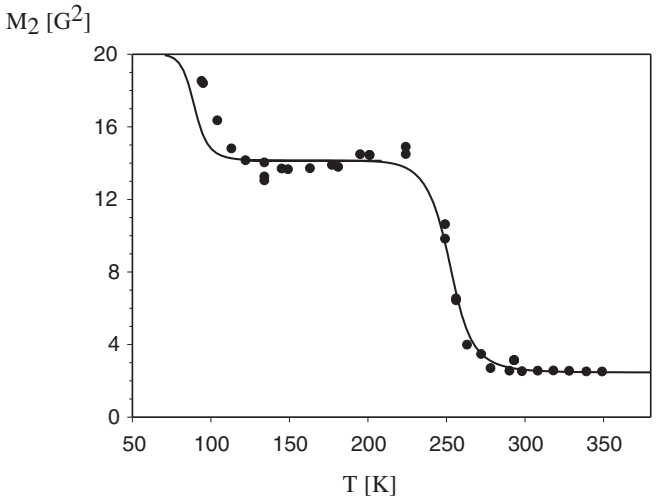

Figure 10. The temperature dependence of the ^{1}H NMR line second moment for $Gu_3Sb_2Br_9$.

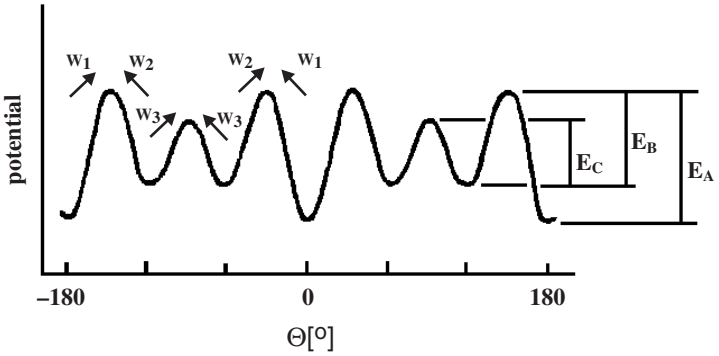

Figure 11. The shape of the potential energy corresponding to the model for the reorientation of the guanidinium cation in $Gu_3Sb_2Br_9$ contributing to the T_1 value at low temperatures (for one of three cations, type II).

at a constant value of the order of 2.5 G^2. It should be noted that this temperature behaviour of M_2 is generally similar to those observed in the case of the chlorine analogue [20]. The small values of M_2 above 275 K may suggest almost isotropic reorientation of the whole guanidinium cation. Analysis of the temperature dependence of the second moment can be performed on the basis of the BPP formula:

$$M_2 = M_2^{\mathrm{II}} + \left(M_2^{\mathrm{I}} - M_2^{\mathrm{II}}\right)\frac{2}{\pi}\tan\left(\gamma\sqrt{M_2}\tau_c\right) \tag{7}$$

where $\tau_c = \tau_0 \exp(E_a/RT)$; M_2^{I} and M_2^{II} are the second-moment values before and after the onset of a given motion, respectively. The reduction of the second moment due to the C_3 reorientations of the guanidinium cation can be described by the known formula

$$\Delta M_2 = \frac{3}{2}\frac{1}{\gamma^2}C \tag{8}$$

where C is the relaxation constant. The solid line in figure 10, exhibiting two second-moment reduction steps, was fitted using the dynamical parameters found in the T_1 relaxation time

experiments (table 6). It should be noted that the 2:1 proportion of the two different kinds of guanidinium cations is consistent with the T_1 relaxation experiment. The second-moment reduction at about 90 K is roughly twice smaller than that at about 250 K.

3.5. Discussion

The guanidinium analogues $Gu_3Sb_2Cl_9$ and $Gu_3Sb_2Br_9$ appear to be isomorphic at room temperature (phase II). The characteristic feature of these two compounds is the presence of the layer anionic structure, $(Sb_2X_9^{3-})_\infty$, in the crystal lattice. The two crystallographically independent guanidinium cations are placed either between the layers (cations of type I) or in the voids of the anionic layers (cations of type II). Since the two kinds of cations possess different environments in the crystal lattice they should be characterized by various freedoms of motion. The cations of type II are connected to the halogen atoms more loosely than those of type I; as a consequence they are dynamically disordered even at low temperatures. The present x-ray studies on $Gu_3Sb_2Cl_9$ and $Gu_3Sb_2Br_9$ crystals reveal quite similar dynamic behaviour of the cations of type II in the structure. The structural and dynamical similarities of the guanidinium crystals studied are reflected in their physical properties. In order to compare the $Gu_3Sb_2Cl_9$ and $Gu_3Sb_2Br_9$ crystals, several points should be discussed:

(i) the phase situation and mechanism of the phase transition;
(ii) the dielectric relaxation process;
(iii) the molecular dynamics of the guanidinium cations on the basis of the proton magnetic resonance studies.

(i) The dilatometric and calorimetric studies reveal one structural phase transition in $Gu_3Sb_2Br_9$ at high temperatures—at 450 K. This bromine analogue undergoes a phase transition that is clearly of first order type. The transition entropy, ΔS_{tr}, accompanying the phase transition at 450 K in $Gu_3Sb_2Br_9$ is extremely large—of the order of 51 J K^{-1} mol^{-1}. It should be taken into account that the observed effect ought to be related to the dynamics of the three guanidinium cations. Assuming that the three cations simultaneously contribute to the mechanism of the phase transition, the entropy effect per cation is equal to about 17 J K^{-1} mol^{-1}. This value is frequently encountered in the ionic crystals with plastic phases. In the title crystal the small, symmetric organic cations should have a large degree of orientational freedom, whereas the anionic sublattice (two-dimensional layers) seems to be rigid even at high temperatures. The observed entropy effect may be explained in terms of isotropic rotations of the cations, resulting in orientational disorder as in plastic phases of molecular crystals [23]. Such a situation was also observed in numerous ionic salts, e.g. various methyl-substituted ammonium cations with simple monovalent inorganic anions such as ClO_4^- [24], NO_3^- [25], BF_4^- [26], SCN^- [27], and in compounds containing bulky symmetric cations—piperidinium [28], pyrrolidinium [29], trimethylammonium [30] and analogous inorganic anions. It should be noted that the shape of the dielectric response (see figure 6) in the vicinity of II $\rightarrow$ I phase transition at 435 K does not resemble that encountered in crystals with typical high temperature plastic phases. The guanidinium cations are endowed with relatively small electric dipole moments, so the releasing of isotropic motion leads to a relatively small change in the dielectric increment ($\Delta\epsilon$). As a consequence, a possible significant defect contribution to the complex electric permittivity can cause a falsification of the real shape of the dielectric response. It should be added that although the two crystals are isomorphic at room temperature, their phase situation is substantially different. The chlorine analogue does not experience any solid–solid phase transition up to the melting point.

(ii) Both guanidinium analogues reveal a low frequency dielectric relaxation (the kilohertz—the chlorine analogue [31]—and megahertz—the bromine analogue—frequency regions) at low temperatures well described by a Debye-type relation. This means that we deal with one dielectric relaxator, which is in agreement with the x-ray data indicating one type of cation (type II) with significant dynamical disorder. It should be stated that the two compounds show nearly identical low frequency dielectric responses below room temperature.

There are three features characterizing the dielectric response of $Gu_3Sb_2Br_9$, namely a small value of the dielectric increment $\Delta\epsilon = (\epsilon_0 - \epsilon_\infty)$ (the value of ϵ_0 being almost independent of temperature), a slight decrease on cooling and the value of ϵ_∞ decreasing with temperature lowering. The small magnitude of the dielectric increment indicates a low value of the dielectrically active dipole moment. This dipole moment is undoubtedly connected with the reorienting guanidinium cations, which are evidently distorted (see table 3). The non-distorted cations have the D_{3h} symmetry and their reorientation around the axis perpendicular to the molecule plane (the C_3-type motion) would not make any contribution to the dipolar polarizability. Moreover the model of cationic motion should take into consideration the fact that the largest value of $\Delta\epsilon_c$ is observed perpendicularly to the cleavage plane (the $\boldsymbol{ab}$-plane), i.e. parallel to the axis of the reorientation of the cation. This means that the motion of the dipolar cation is more complex than exclusively the postulated C_3-type reorientation.

The character of the changes of ϵ_0 with temperature may be explained in terms of dipolar interactions. The dipole–dipole interactions contributing to the electric polarizability of $Gu_3Sb_2Br_9$ seem to play a minor role since ϵ_0 is almost independent of temperature. In fact these interactions are certainly weaker than those in the case of $Gu_3Sb_2Cl_9$ where an increase of ϵ_0 is observed with temperature decreasing [31].

On the other hand we cannot exclude the contribution of the anionic sublattice to the dipolar polarizability of the crystal. It is well known that halogenoantimonate(III) salts, characterized by the anionic layer structure, mainly those with the $(Sb_2X_9^{3-})$ composition, are strongly polarizable. It is reflected in the relatively large magnitude of ϵ_∞, exceeding 10–12 units.

The dependence of ϵ_∞ on the temperature points to an additional high frequency relaxation process. The dispersion and absorption of the electric permittivity, to be ascribed to this process, should appear at markedly higher frequencies. The well shaped maxima of ϵ'' in the low frequency region (see figure 5) indicate a pronounced separation of the two processes in the frequency domain. The effects related to the polarization of the anionic structure should be observed at significantly higher frequencies, which could support the participation of the anionic structure in the dipolar polarization of $Gu_3Sb_2Br_9$.

The estimated dielectric relaxation times are two orders shorter for bromine crystal than for the chlorine one. This is consistent with the fact that the electric dipole–dipole interactions are weaker in the bromine crystal. Also the activation energy of the dielectric relaxation is insignificantly lower for $Gu_3Sb_2Br_9$, which is in agreement with the conclusion drawn above. This may suggest that the steric hindrance for the rotating guanidinium cation is probably bigger in the case of $Gu_3Sb_2Cl_9$.

(iii) The temperature characteristics of the spin–lattice relaxation time, T_1, for the two guanidinium compounds reveal significant similarity at temperatures above 80 K—namely, the existence of two well shaped and distinctly separated minima (at 215 and 400 K, chlorine, for 60 MHz and at 153 and 372 K, bromine, for 90 MHz). Since for $Gu_3Sb_2Cl_9$ the measurements were carried out exclusively down to 80 K, the two minima were ascribed to two structurally non-equivalent cations performing the C_3 type of motion [20]. The appearance of the subsequent low temperature minimum in the T_1 versus temperature curve at 82 K for $Gu_3Sb_2Br_9$ means that these results cannot be interpreted using the model proposed by Grottel [20] for the isomorphic crystal $Gu_3Sb_2Cl_9$. Dynamical non-equivalence of the guanidinium cations

in $Gu_3Sb_2Br_9$ is reflected both in the second-moment and in the spin–lattice relaxation experiments. The observed two-step reduction of the second moment confirms the existence of two different dynamic processes assigned to the two kinds (I and II) of cations.

The high temperature minimum on the T_1 versus temperature curve found for $Gu_3Sb_2Br_9$ (similar to that for $Gu_3Sb_2Cl_9$) is ascribed to cations of one type (two thirds of all cations) performing the C_3 type of motion. The two low temperature minima, however, are assigned to the dynamics of cations of the second type (a third of all cations). This dynamics is related to the complex pseudo-C_6 type of motion. The model proposed by Ito [21], explaining the molecular dynamics in the pyridinium derivative, $PyHAuX_4$ (X = Cl, Br), was applied successfully for the description of the C_6' motion of the 2-aminopyridinium cations in the 2-$NH_2PyHSbX_4$ (X = Cl, Br) salts [32].

It should be emphasized that the ^{1}H NMR results at high temperatures clearly indicate a change in the motional state of the cations at 450 K. In fact the onset of the isotropic motion of all cations is believed to occur above 450 K, which is consistent with the thermal studies. Similarly to in the case of the above-mentioned ionic crystals, the self-diffusion attributable to the small guanidinium cations is suggested to appear above 450 K.

3.6. Conclusions

(i) The $Gu_3Sb_2Br_9$ and $Gu_3Sb_2Cl_9$ crystals are built of two-dimensional anionic layers ($Sb_2X_9^{3-}$) and non-equivalent guanidinium cations (two kinds).

(ii) The $Gu_3Sb_2Br_9$ crystal undergoes a high temperature structural phase transition at 450 K of first-order type.

(iii) The low frequency dielectric relaxation process at low temperatures found in $Gu_3Sb_2Br_9$ is assigned to the dynamics of one out of three guanidinium cations, which are placed inside the voids of the polyanionic layers.

(iv) The non-equivalence of the two kinds of guanidinium cations in $Gu_3Sb_2Br_9$ is confirmed by the ^{1}H NMR relaxation time, T_1, and second-moment, M_2, results.

Acknowledgment

This work was supported by the Polish State Committee for Research (project register number 3T09A 023 26).

References

[1] Jakubas R and Sobczyk L 1990 *Phase Transit.* **20** 163
[2] Varma V, Bhattacharjee R, Vasan H N and Rao C N R 1992 *Spectrochim. Acta* A **48** 1631
[3] Sobczyk L, Jakubas R and Zaleski J 1997 *Pol. J. Chem.* **71** 265 and references cited therein
[4] Jakubas R, Krzewska U, Bator G and Sobczyk L 1988 *Ferroelectrics* **77** 129
[5] Zaleski J and Pietraszko A 1996 *Acta Crystallogr.* B **52** 287
[6] Kawai T, Takao E, Shimanuki S, Iwata M, Miyashita A and Ishibashi Y 1999 *J. Phys. Soc. Japan* **68** 2848
[7] Jakubas R 1989 *Solid State Commun.* **69** 267
[8] Lefebvre J, Carpentier P and Jakubas R 1995 *Acta Crystallogr.* B **51** 167
[9] Józków J, Bator G, Jakubas R and Pietraszko A 2001 *J. Chem. Phys.* **114** 7239
[10] Kuok M H, Ng S G, Tan I S, Rang Z I, Iwata M and Ishibasi Y 1998 *Solid State Commun.* **108** 159
[11] Jakubas R, Ciunik Z and Bator G 2003 *Phys. Rev.* B **64** 024103
[12] *KUMA 1996 KUMA Diffraction Software. Version 8.1.0 and 8.1.1, KUMA Diffraction, Wrocław, Poland*
[13] *Oxford Diffraction 2001, CrysAlis 'CCD' and CrysAlis 'RED', Oxford Diffraction (Poland) Sp. z o.o, Wrocław, Poland*

[14] Sheldrick G M 1997 *SHELX-97 (1997) Program for Solution and Refinement of Crystal Structure* University of Göttingen, Germany
[15] Sheldrick G M 1990 *SHELXTL (1990) Siemens Analytical X-ray Instruments Inc.* Madison, Wisconsin, USA
[16] Zaleski J and Pietraszko A 1994 *Z. Naturf.* a **49** 895
[17] Cole K S and Cole R H J 1941 *Chem. Phys.* **9** 341
[18] Ciąpała P, Zaleski J, Bator G, Jakubas R and Pietraszko A 1996 *J. Phys.: Condens. Matter* **8** 1957
[19] Jakubas R, Bator G, Ciąpała P, Zaleski J, Baran J and Lefebvre J 1995 *J. Phys.: Condens. Matter* **7** 5335
[20] Grottel M, Pająk Z and Zaleski J 2001 *Solid State Commun.* **120** 119
[21] Ito Y, Asaji T, Ikeda R and Nakamura D 1988 *Ber. Bunsenges. Phys. Chem.* **92** 885
[22] Medycki W and Jakubas R 2002 *Solid State Nucl. Magn. Reson.* **21** 44
[23] Sherwood J N (ed) 1979 *The Plastically Crystalline State* (New York: Wiley)
[24] Ishida H, Ikeda R and Nakamura D 1987 *Bull. Chem. Soc. Japan* **60** 467
[25] Ishida H, Ikeda R and Nakamura D 1985 *J. Chem. Soc. Faraday Trans.* **281** 963
[26] Ishida H, Hayama N and Ikeda R 1992 *Chem. Lett.* 1333
[27] Tanabe T, Ikeda R and Nakamura D 1991 *J. Chem. Soc. Faraday Trans.* **87** 987
[28] Ono H, Ishimaru S, Ikeda R and Ishida H 1997 *Chem. Phys. Lett.* **275** 485
[29] Ono H, Ishimaru S, Ikeda R and Ishida H 1999 *Bull. Chem. Soc. Japan* **72** 2049
[30] Kuchitsu K, Ono H, Ishimaru S, Ikeda R and Ishida H 2000 *Phys. Chem. Chem. Phys.* **2** 3883
[31] Zaleski J, Jakubas R, Bator G and Baran J 1994 *J. Mol. Struct.* **325** 95
[32] Kulicka B, Jakubas R, Bator G, Ciunik Z and Medycki W 2004 *J. Phys.: Condens. Matter* **16** 8155